

Original Article

Cite this article: Peacock DCP, Sanderson DJ, and Magán M (2023) Superposed fracture networks. *Geological Magazine* **160**: 1817–1831. <https://doi.org/10.1017/S0016756823000730>

Received: 31 August 2023

Revised: 26 October 2023

Accepted: 6 November 2023

First published online: 4 December 2023

Keywords:

fractures; veins; joints; geometry; topology; timing

Corresponding author:

D.C.P. Peacock;

Email: peacock@uni-goettingen.de

Superposed fracture networks

D.C.P. Peacock¹ , D.J. Sanderson² and M. Magán³

¹University of Göttingen, Göttingen, Germany; ²Ocean and Earth Science, University of Southampton, National Oceanography Centre, Southampton, SO14 3ZH, UK and ³Departamento de Geología, Universidad de Oviedo, Oviedo, EU, Spain

Abstract

The concept of *superposed fracture networks* consisting of different generations, and often types, of fractures that have developed sequentially is discussed. Superposed networks can consist of different types of extension or shear fractures, and each fracture may abut, cross or follow (reactivate) earlier fractures. An example of a superposed fracture network in Liassic limestones in Somerset, UK, is presented, which comprises two sets of veins and a later joint network. The veins develop as damage zones around faults, with veins of the later set crossing or trailing along the earlier set. The later joints either cross-cut the earlier veins or reactivate them, the latter being common for the thicker (more than about 5 mm) veins. The veins and joint networks have markedly different geometries and topologies. The veins are spatially clustered and are typically dominated by I-nodes, while the joints are more evenly distributed and tend to be dominated by Y-nodes. The combined network of veins and joints at Lilstock is dominated by X-nodes because so many joints cross-cut the earlier veins. Understanding the development of superposed fracture networks leads to better understanding of the kinematic, mechanical, tectonic and fluid flow history of rocks.

1. Introduction

Many networks have been shown to be the result of several generations (and types) of fractures (e.g., Hancock, 1985; Hanks *et al.*, 2004; Nortje *et al.*, 2011). We term these *superposed fracture networks*. The characterization and description of such networks require careful identification of different types and generations of fractures. Measurement and statistical analysis can and should be designed to recognize these differences and avoid confusing and grouping of disparate structures. In this paper, we discuss how fracture types and generations can be incorporated into the geometrical and topological analysis of a network, as opposed to the analysis of individual fractures.

A *superposed fracture network* is defined here as a system that consists of more than one generation of intersecting fractures. The component fractures could be the same type, such as one set of veins that abuts, crosses or reactivates an earlier set of veins (Fig. 1a). A superposed fracture network may also include different types of fractures, such as a fault with a network of veins in a damage zone (one generation of fractures) superposed by a network of later joints (Fig. 1b). The fractures forming a component part of a superposed fracture network may either be a simple set of fractures or a network of several fracture sets. The key feature of a superposed fracture network is that it consists of different generations of fractures, as indicated by abutting, crossing and reactivation relationships. We use the terms *superposed deformation* (e.g., Lindström, 1961; Treagus, 1995) and *superposed folds* (e.g., Weiss, 1959) as precedents for using the term *superposed* to describe fracture networks. Various authors have used the term *superposed fractures* (e.g., Nekrasov, 1975; Lewis *et al.*, 2023), *superposed veins* (e.g., Reinhardt & Davison, 1990; d'Ars & Davy, 1991) and *superposed faults* (e.g., Stanley, 1974; Gorodnitskiy *et al.*, 2009). The term *superimposed* has also been used to describe different generations of brittle structures (e.g., Gonzalo-Guerra *et al.*, 2023).

The aims of the paper are (1) to define and illustrate the term superposed fracture networks and (2) to show the key geometric observations necessary to understand the development of superposed fracture networks and to interpret routinely measured parameters. Such an approach is also a necessary prerequisite to subsequent tectonic, kinematic and mechanical interpretation of the fractures and to understanding how the networks may contribute to the physical and engineering properties of the rock mass. For example, connectivity of a network (e.g., Manzocchi 2002; Sanderson and Nixon, 2018) is fundamental to both the flow of fluids (Lee *et al.*, 1993; Berkowitz *et al.*, 2000) and the strength of the rock mass (e.g., Dershowitz, 1984; Odling, 1997).

Analysis is presented of a network of veins and joints on a Liassic limestone bedding plane at Lilstock, Somerset, UK (51°12'08.9''N 3°10'06.0''W; Fig. 2). This location was chosen because of the high quality of the exposure and because it shows key features that enable relative ages of the network components to be determined (Peacock and Sanderson, 1999; Peacock, 2001). The

© The Author(s), 2023. Published by Cambridge University Press. This is an Open Access article, distributed under the terms of the Creative Commons Attribution licence (<http://creativecommons.org/licenses/by/4.0/>), which permits unrestricted re-use, distribution and reproduction, provided the original article is properly cited.



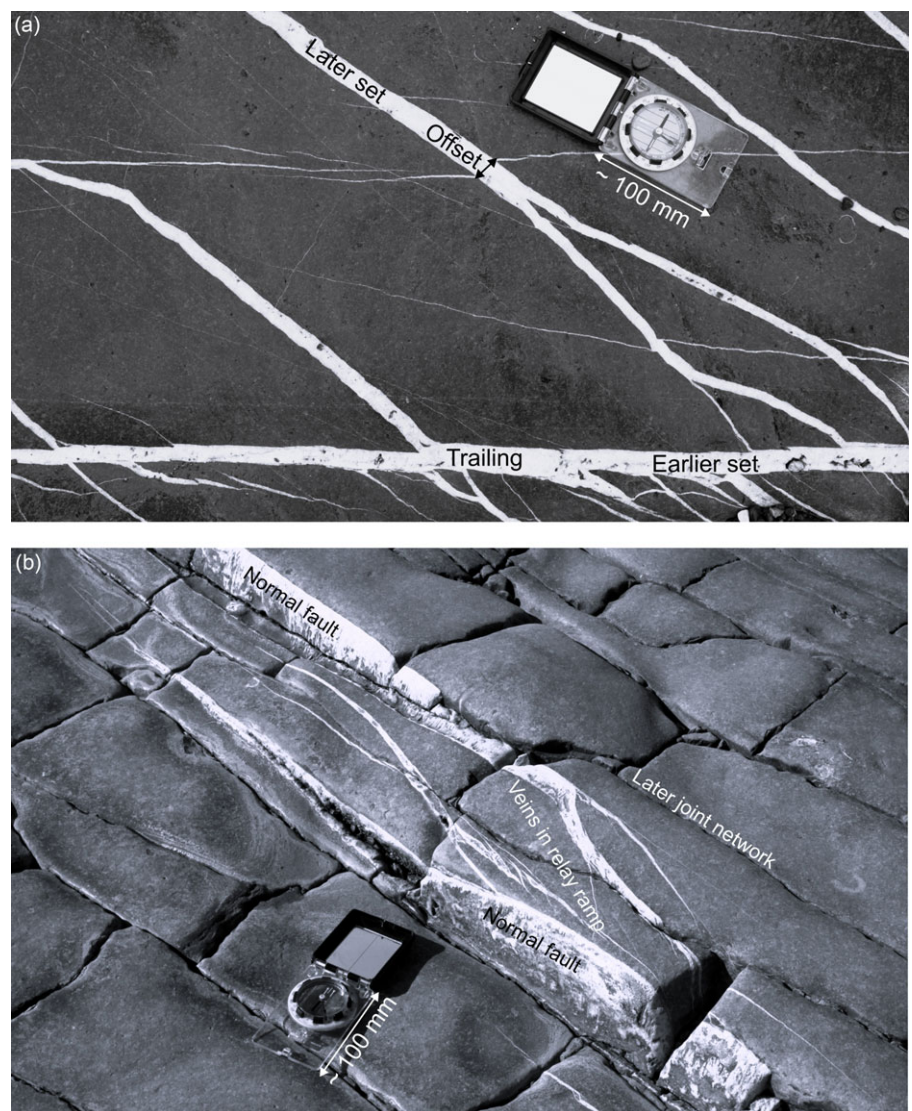


Figure 1. (Colour online) Examples of different types of superposed fracture networks. (a) Two sets of calcite veins of different ages. Liassic limestone at Lilstock. View vertically downwards. (b) Normal fault zone with a network of calcite veins in a damage zone (one generation of fractures) superposed by a network of later joints. Liassic limestone at East Quantoxhead (51°11'27''N, 3°14'15''W). View downwards at approximately 45° to the NW.

superposed fracture networks have been mapped using drone images and GIS to record fracture type, geometry (orientation and length) and topology. This analysis is augmented with key field observations, especially at fracture intersections, to establish the sequence of fracture development. This enables the evolution of superposed fracture network to be determined.

Note that here we use the noun *fracture* as a general term for planar brittle structures, including faults, veins and joints. More specific terms are used as appropriate. Considering brittle deformation of rock in terms of *superposed fracture networks* is important because the emphasis on determining the age relationships, based on geometric and topological relationships, leads to improved understanding of the development of the structures. Also note that the use of 'younging tables' to record relative ages of structures has been suggested (e.g., Potts & Reddy, 1999, 2000), but we do not use that approach in this paper.

2. Geological setting of the Lilstock study area

The study location is on the coast between Lilstock and Hinkley Point, Somerset, UK, on the south side of the Bristol Channel Basin (e.g., Van Hoorn, 1987; Fig. 2). The area underwent Mesozoic N-S

extension and Cenozoic N-S contraction (e.g., Dart *et al.*, 1995, Glen *et al.*, 2005). Three main groups of structures can be identified in the Liassic rocks exposed on the Somerset coast (e.g., Dart *et al.*, 1995): (1) ~095°-striking normal faults and associated calcite veins, with some of these showing evidence of both sinistral and dextral reactivation at Lilstock (Peacock & Sanderson, 1999; Rotevatn & Peacock, 2018); (2) E-W-striking thrusts, strike-slip faults that are conjugate about ~N-S and reverse-reactivation of the largest 095°-striking normal faults, all with associated calcite veins; and (3) joints (e.g., Peacock, 2001).

The exposure consists of a bedding plane near the base of the Liassic (Lower Jurassic) sequence of interbedded limestone and shales, approximately 0.3 m thick and dipping a few degrees to the north (Fig. 3). 095°-striking normal faults and sinistral strike-slip faults occur at the location. The vein network consists of two distinct sets formed at different times under different stress orientations. Stylolites occur between some of the *en echelon* veins, with shear along some stylolites causing the veins to develop as pull-aparts (Willemse *et al.*, 1997). It is more difficult to divide the joint network into distinct sets based on their orientation, and they probably formed in an evolving stress during exhumation (Rawnsley *et al.*, 1998).

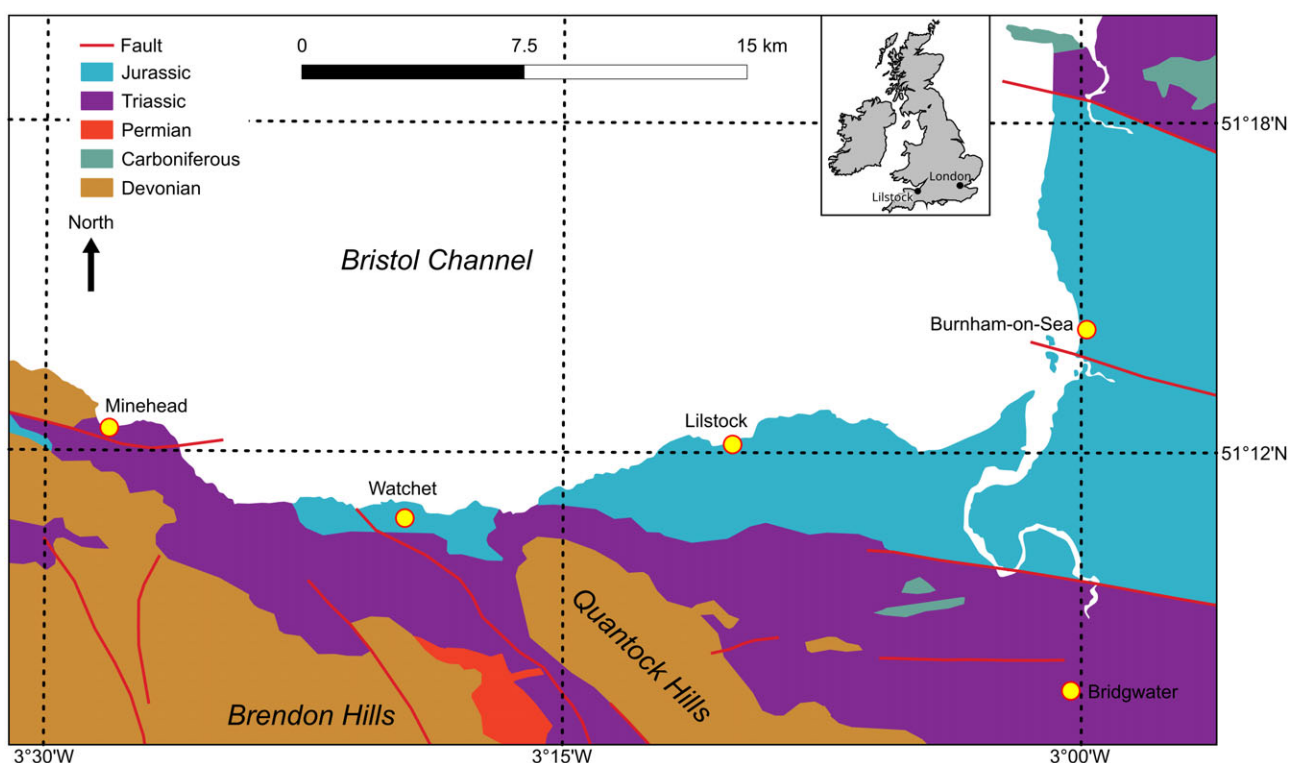


Figure 2. (Colour online) Geological map of western Somerset, showing the location of the study site at Lilstock. The geology is from the British Geological Survey 1:625,000 scale map of the UK. Reproduced with the permission of the British Geological Survey ©NERC. All rights Reserved.

This location was used by Ryan *et al.* (2000) to demonstrate a method for the measurement and display of fracture spacing and orientation from maps of fracture networks. A map of veins at this location was also used by Belayneh *et al.* (2006) to demonstrate how a percolation approach can be used to predict vein connectivity. Willemse *et al.* (1997) and Sanderson and Peacock (2019) use examples of veins within approximately 300 m of the exposure to demonstrate aspects of vein development. Exposures on the coast, approximately 2.1 km west of the location, have been used to analyse joint patterns (e.g., Passchier *et al.*, 2021).

We use this location to: (1) recognize different fracture types, (2) determine the geometries and topologies of the different fracture types, (3) interpret the age relationships and development of the superposed fracture networks and (4) determine the effects of pre-existing fractures on the development of later fractures. Note that here the emphasis is on the veins and joints rather than faults and stylolites.

3. Methods

3.a. Data collection

A drone was flown at a height of ~3 m above the exposure to collect 577 vertical photographs, each photograph being 4864 × 3648 pixels. They cover an area ~96 m E-W and 20.6 m N-S. The flight was planned using the DroneDeploy application, with the images having ~70% overlap to allow photogrammetry. Agisoft Metashape was used to create an orthomosaic, with each pixel being ~2 mm × 2 mm, and a digital elevation model (DEM) with pixel sizes of ~4 mm × 4 mm.

3.b. Mapping

The orthomosaic and DEM were analysed using QGIS (version 3.26.0). The traces of fractures were digitized at scales of up to 1:2, with the 'enable snapping' and 'enable snapping on intersection' functions switched on. The following four types of fracture trace were digitized:

- *Faults*: identified by lateral displacement of pre-existing veins seen on the orthomosaic and by height differences on the bedding plane highlighted by using hill-shading of the DEM.
- *Veins*: appear as white or light brown lines on the orthomosaic.
- *Joints*: appear as black or dark lines on the orthomosaic.
- *Joints along veins*: fracture traces that consist of both veins and joints (i.e., joints following and reactivating veins).

These classes enable analysis of all of the fractures that are veins (by combining *veins* and *joints along veins*) and of all of the fractures that are joints (by combining *joints* and *joints along veins*). The resolution of the imagery means that we only consider veins or joints with lengths greater than ~4 mm and veins with apertures of greater than ~2 mm.

3.c. Problems and ambiguities

Various problems and ambiguities were encountered when digitizing the fractures. While it was generally simple to identify faults with lateral offsets of a few millimetres or vertical offsets of a few centimetres, it was more difficult to identify smaller displacements. It was also difficult to accurately identify the tips of faults,

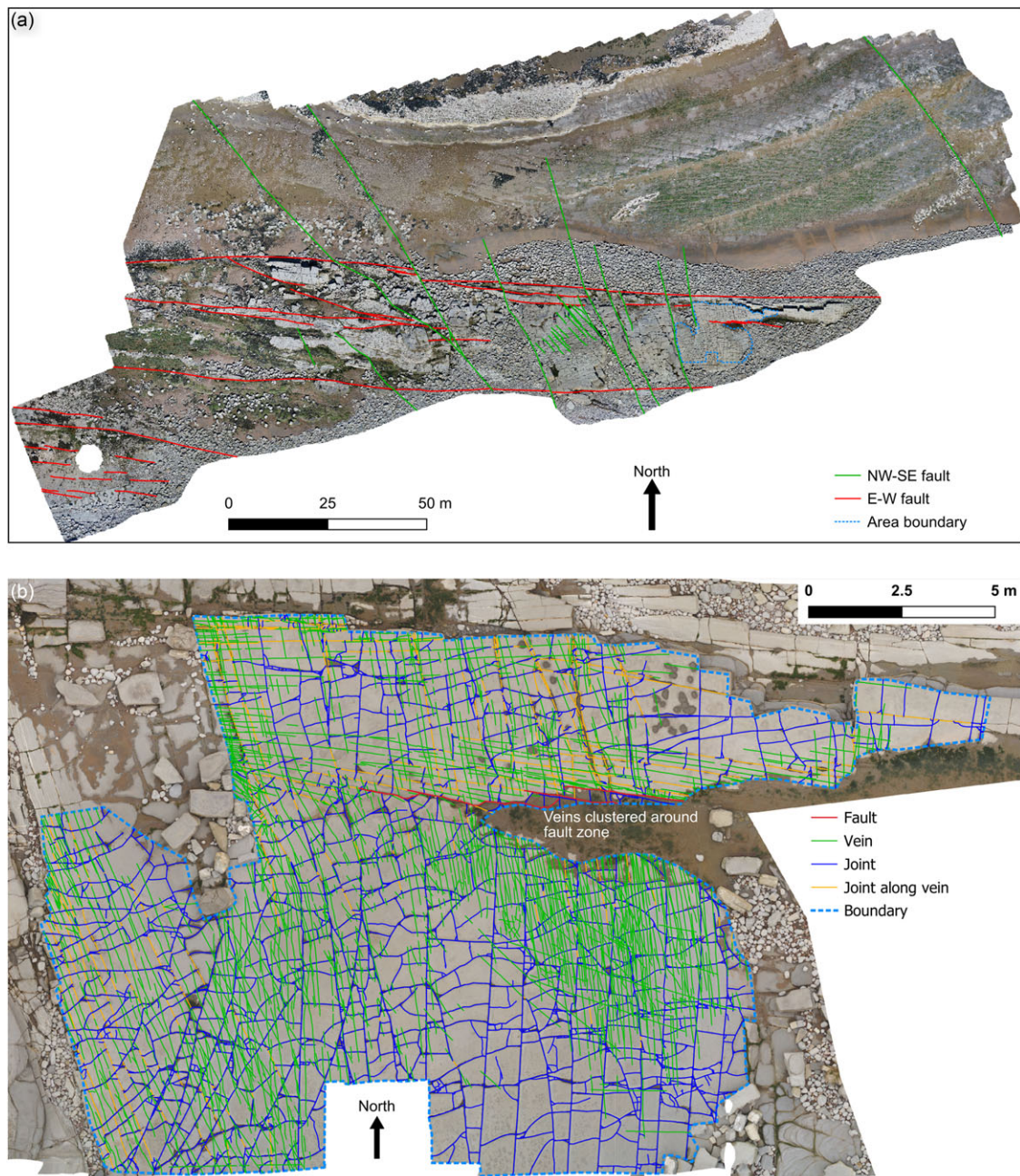


Figure 3. (Colour online) (a) Overview map of the area, based on an orthomosaic (pixel size $\sim 7 \text{ mm} \times 7 \text{ mm}$) made using photographs taken using a drone flown $\sim 20 \text{ m}$ above the surface. Faults have been mapped from the orthomosaic, with \sim E-W-striking faults probably having normal displacements, although some strike-slip is likely (Rotevatn & Peacock, 2018). The \sim NW-SE-striking faults generally show dextral displacements of up to $\sim 1 \text{ m}$. (b) Larger-scale view of the mapping area, with structures mapped from an orthomosaic (pixel size $\sim 2 \text{ mm} \times 2 \text{ mm}$).

where displacements decrease to sub-resolution scales, especially where such faults pass laterally into veins apparently with only opening-mode displacements. The faults are mineralized and joints tend to follow portions of those faults, but they have been mapped simply as faults.

Some of the veins in the area have apertures of up to about 70 mm. The area also shows veins with centimetre-scale spacings, metre-scale lengths and sub-millimetre-scale apertures, these being formed by a process termed *crack-jump* by Caputo and Hancock (1998). It is therefore difficult to see the smaller veins at the resolution of the orthomosaic. See Snow (1970), Marrett (1996)

and Forstner and Laubach (2022) for descriptions of fracture apertures in rock. As with the faults, it is particularly difficult to see the low-displacement parts of the veins, making it hard to identify vein tips and therefore to determine the connectivity of the veins. Veins are typically segmented, with many veins being composites of linked segments (e.g., Vermilye & Scholz, 1995). It can be difficult to decide whether to digitize two stepping veins or a single composite vein, which may influence the numbers of traces mapped but has little effect on the sum of their lengths (Table 1). Another ambiguity is that some later veins intersect, follow and re-emerge from earlier veins. Such trailing veins were digitized as

Table 1. Data for fracture trace lengths for the superposed fracture network at Lilstock. Mapped area = 227.358 m². *Intensity* is mean length per unit area. Note that the values for 'Joints' includes the values for 'Joints following Set A veins' and 'Joints following Set B veins'. 6.7% of the length of joints follows Set A and 12.6% of the length of joints follows Set B. 23.8% of the length of Set A is followed by later joints, while the 11.7% of the length of Set B is followed by later joints

Set	<i>n</i>	Total length (m)	Intensity (m ⁻¹)	% Total length
Set A veins	1412	279.3	1.23	11.9
Set B veins	2845	1074.6	4.73	45.7
Joints	1881	997.6	4.39	42.4
Joints following Set A veins	118	66.6	0.29	2.8
Joints following Set B veins	265	126.3	0.56	5.4

being two veins intersecting the older vein rather than as a single vein. We consider this preferable to trying to identify and digitize each case of trailing.

The imagery has a pixel size of ~ 2 mm × 2 mm. The traces of all of the fracture types identified can form anastomosing patterns, sometimes making it difficult to determine the start and end points of each anastomosing fracture, which may influence such parameters as the length distributions of the fracture networks. These side-stepping and anastomosing patterns are mostly near or below the resolution of the imagery and are not considered in construction of the larger scale (>>4 mm) networks represented and analysed in this paper. We only consider total trace lengths for the different fracture types (Table 1) rather than their scaling relationships.

The veins have widths of up to several millimetres, and many of the joints also have mm-scale apertures, probably partly because of weathering. The intersection points (nodes) are therefore really areas rather than points, but those intersection areas are small relative to the scale of the mapping.

While these various issues created some problems with digitizing and interpretation, the ambiguous traces comprise a small percentage of the total fracture population. We consider them to not influence the main observations or results presented in this paper.

3.d. Ground-truthing

The mapping using the orthomosaic and DEM was undertaken with the benefit of numerous previous visits to the location. It was necessary, however, to ground-truth the results, check the relationships between different types and sets of fractures, and take higher-resolution photographs of key features (i.e., from nearer to the exposure than the ~3 m height flown by the drone).

4. Relationships between superposed fractures

We identify four common types of relationships between pairs or sets of fractures of different ages, with the relationships giving information about the relative ages of the fractures (Peacock *et al.*, 2018):

- *Cross-cutting*: where later fractures cross and displace earlier fractures. A fault that crosses and displaces another fault will be the younger of the two (e.g., Chen, 2013). The relative ages of crossing veins can commonly be determined by the displacement patterns (Fig. 4a) or by the pattern of mineral infills (e.g., Craw *et al.*, 2010). The lack of measurable displacements or mineral fill mean that it is difficult to determine the relative ages of crossing joints.

- *Abutting*: where a fracture meets another fracture at an intersection line or point. A later joint commonly abuts an earlier joint (Fig. 4b; e.g., Rives *et al.*, 1994). Note, however, that an earlier fault can be displaced by, and therefore abut, a later fault (e.g., Nixon *et al.*, 2014). Also note that abutting relationships can be caused by the splaying of one fracture off another, with the two fractures being synchronous (e.g., Biddle & Christie-Blick, 1985).
- *Trailing*: where two new fractures are connected through an older fracture, with renewed displacement occurring on the older fracture (Fig. 4c, d). Trailing faults are illustrated by Nixon *et al.* (2014), Phillips *et al.* (2018) and by Deng and McClay (2021), and trailing veins are illustrated by Virgo *et al.* (2013, Fig. 12c).
- *Reactivating*: the term *reactivation* is typically used for renewed displacement on a *fault* that has undergone a prolonged period of inactivity (e.g., Shephard-Thorn *et al.*, 1972; Sibson, 1985). Here, however, we generalize the term for other fracture types, such as where a joint follows and causes renewed opening along an earlier vein (e.g., Fig. 4e). Such reactivation of fractures has been described for veins (e.g., Ramsay, 1980; Zulauf, 1993; Evans, 1994), dykes (e.g., Drobe *et al.*, 2013) and faulted joints (e.g., Wilkins *et al.*, 2001).

These relationships provide evidence for the relative ages and therefore the superposition of fracture networks. It may also be possible to use non-geometric data to determine superposition, such as mineral paragenesis and radiometric dating of different fracture cements (e.g., Guastoni *et al.*, 2014).

5. Geometries of superposed fracture networks at Lilstock

5.a. Vein networks

The calcite veins show the following characteristics:

- *Orientations*. The mapped veins all dip at ~90° to bedding, which has a gentle dip to the north, with vein strike data shown in Fig. 5a, b. These strike data indicate two sets of veins, one set striking ~ 085° to 115° (Set A, ~18% of data) and another a dominant set striking ~ 145° to 185° (Set B, ~75.5% of data). The sets have a strong and well-defined preferred orientation, with most of the data (~93.5% of data) within these narrow orientation ranges (Fig. 5a). These two sets have been divided in QGIS using cut-offs of 045–125° (Set A) and 125–225° (Set B), with maps shown in Fig. 6a, b. Sets A and B are therefore defined on the basis of fracture type (calcite veins) and orientation.

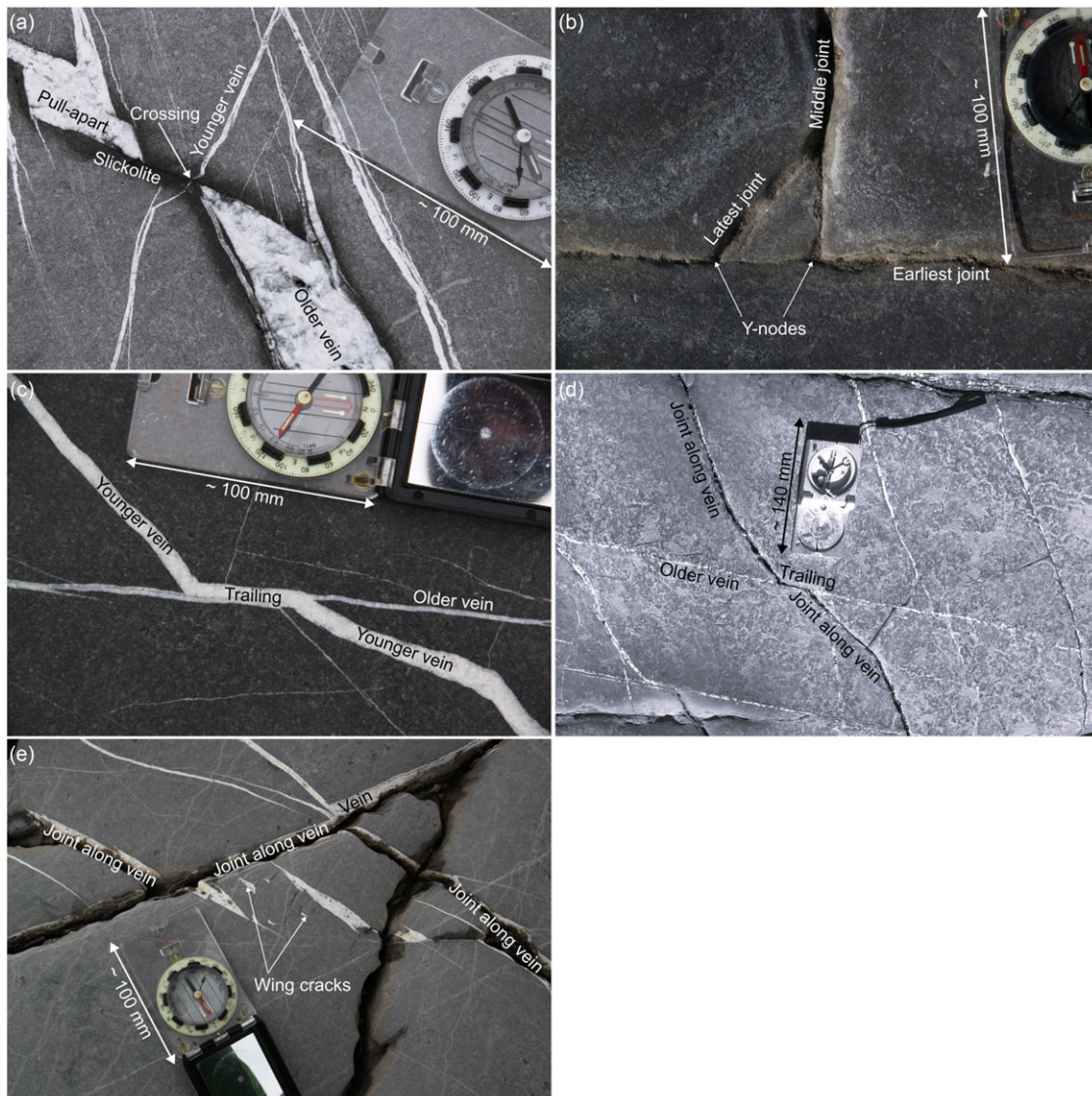


Figure 4. (Colour online) Examples from Liassic limestones at Lilstock of different types of relationships between fractures that give information about their relative ages. All views are approximately vertical downwards. (a) Earlier veins are connected by slickolites to form pull-aparts, with a later vein crossing a slickolite. (b) Abutting joints, with the abutting relationships giving the relative ages of the joints. (c) Trailing calcite veins. (d) Example of joints trailing through a calcite vein. (e) Later joints following and reactivating earlier calcite veins.

- **Apertures.** The calcite veins of both sets typically have apertures of up to ~ 10 mm, although some of the veins in the area have apertures of up to ~ 70 mm. When observed with a hand lens, the calcite appears to be sparry with no visible evidence for crack-seal. Wider veins occur, although joints and weathering along these wider veins tend to make aperture measurements ambiguous. Both sets show veins with apertures that are below the $\sim 2 \text{ mm} \times 2 \text{ mm}$ pixel size of the imagery.
- **Trace lengths.** The maximum trace length measured for Set A is at least 3.844 m, with this longest vein extending to the edge of the mapping area. The maximum trace length measured for Set B is at least 6.32 m, with this longest vein extending to the edge of the mapping area. The shortest measured vein of Set A is at the limits of the drone imagery, and the mean length is $\sim 198 \text{ mm}$ ($n = 1412$). The shortest measured vein of Set B is at the limits of the drone imagery, and the mean

length is $\sim 259 \text{ mm}$ ($n = 2845$). Fracture trace length data are summarized in Table 1. Note, however, that caution is needed with these length measurements, which are likely to be underestimates of true values (see Section 3.c). Set A veins show mean trace lengths per unit area of $\sim 1.2 \text{ m}^{-1}$, and Set B shows mean trace lengths per unit area of $\sim 4.7 \text{ m}^{-1}$ (mapped area = 227.358 m^2).

- **Geometric indicators of kinematics.** Veins in Set A commonly show left-stepping, *en echelon* relationships, indicating a component of \sim E-W dextral shear. *En echelon* patterns are less obvious in Set B, although some appear to show shear fractures and pull-aparts (Willemsse *et al.*, 1997; Sanderson & Peacock, 2019) indicating \sim NNW-SSE sinistral shear.
- **Distributions.** Both vein sets appear to show spatial relationships to faults. Set A are clustered around the \sim E-W-striking faults, with most of the veins of this set occurring in the north of the mapped area (Fig. 6a). Set B is more widely distributed

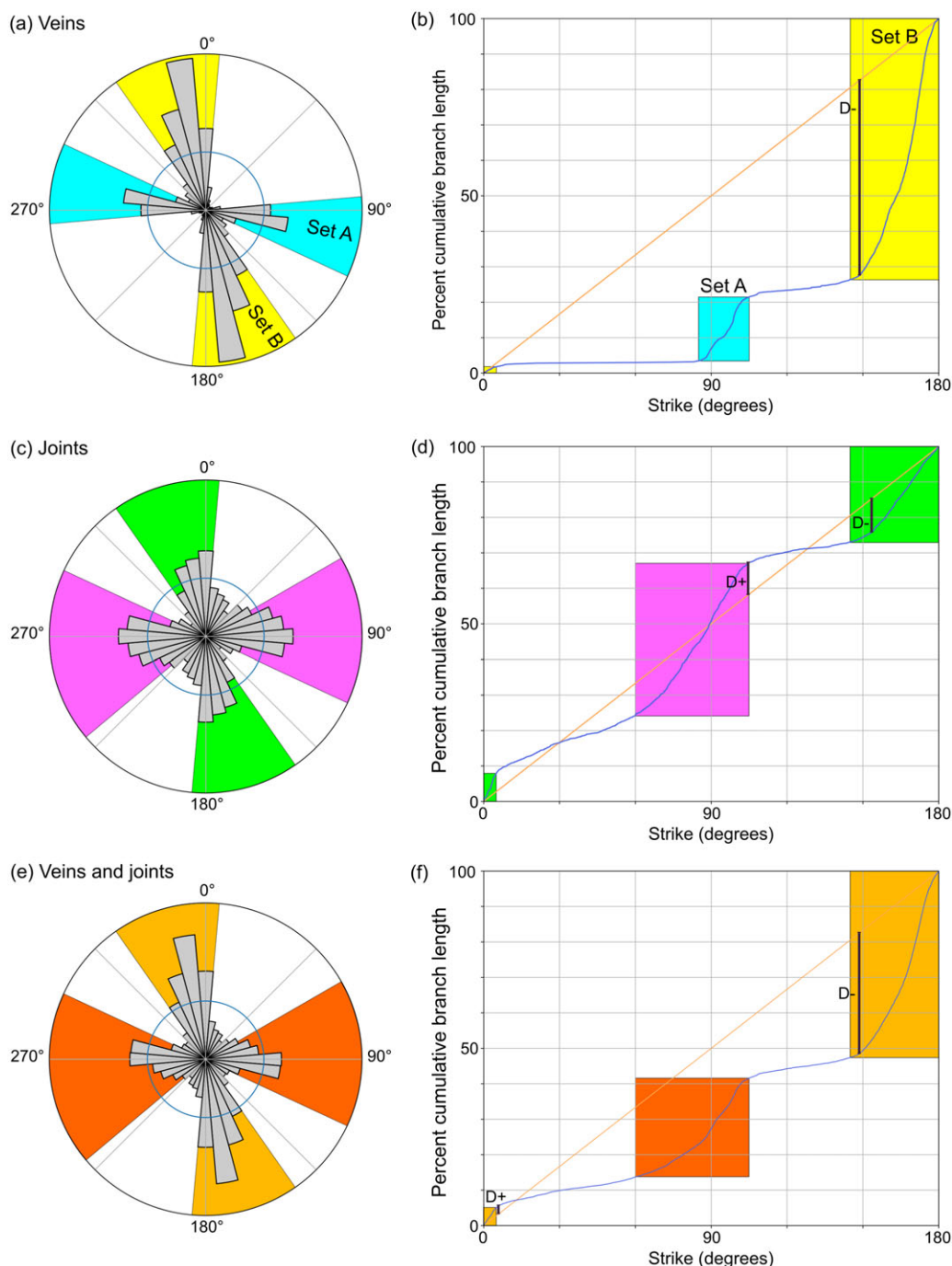


Figure 5. (Colour online) Orientation data for the fractures at Lilstock. (a) Rose diagram, weighted to length and area proportional, for the veins ($n = 4763$). (b) Graph of vein strike vs percentage cumulative branch length for the veins. The straight dashed line, from (0,0) to (180,100), represents a uniform orientation distribution, with deviation of the data from this line providing a useful and unbiased indication of the departure from uniformity (Sanderson & Peacock, 2020). Maximum deviation ($D+$) = 0.05; minimum deviation ($D-$) = - 55.09, $V = 55.14$. The sum $V = |D+| + |D-|$ is independent of the choice of origin, with $V = 0$ representing a perfectly uniform distribution, and $V = 1$ representing a parallel alignment of lines (Sanderson & Peacock, 2020). The data indicate a dominant strike of veins at $\sim 145^\circ$ to 185° (Set B), with a secondary strike of $\sim 085^\circ$ to 115° (Set A). (c) Rose diagram for the joints ($n = 5064$). (d) Graph of vein strike vs percentage cumulative frequency for the joints. $D+ = 9.1$, $D- = - 9.5$, $V = 18.6$, $V^* = 13.26$. The data indicate a wider range of strikes than shown by the veins, with a dominant orientation of $\sim 070^\circ$ to 110° . (e) Rose diagram for the veins and the joints ($n = 9827$). (f) Graph of vein and joint strike vs percentage cumulative frequency for the veins and joints. $D+ = 2.34$, $D- = - 34.11$, $V = 36.45$, $V^* = 44.22$. The data show intermediate behaviour between the vein and the joint data.

in the mapped area (Fig. 6b) but appears to be concentrated along-strike from faults of similar trend (Fig. 3).

- *Relationships between veins.* Some veins of the same set show *en echelon* relationships, with some pull-aparts developed in veins of Set B. Veins of Set B cross-cut or show trailing

relationships with veins of Set A. Some veins of Set B cross-cut other veins of Set B, with \sim NNW-SSE-striking veins appearing to cross-cut \sim N-S-striking veins.

- *Relative ages.* Crossing and trailing relationships suggest that Set A pre-dates Set B. Crossing relationship of veins of Set B

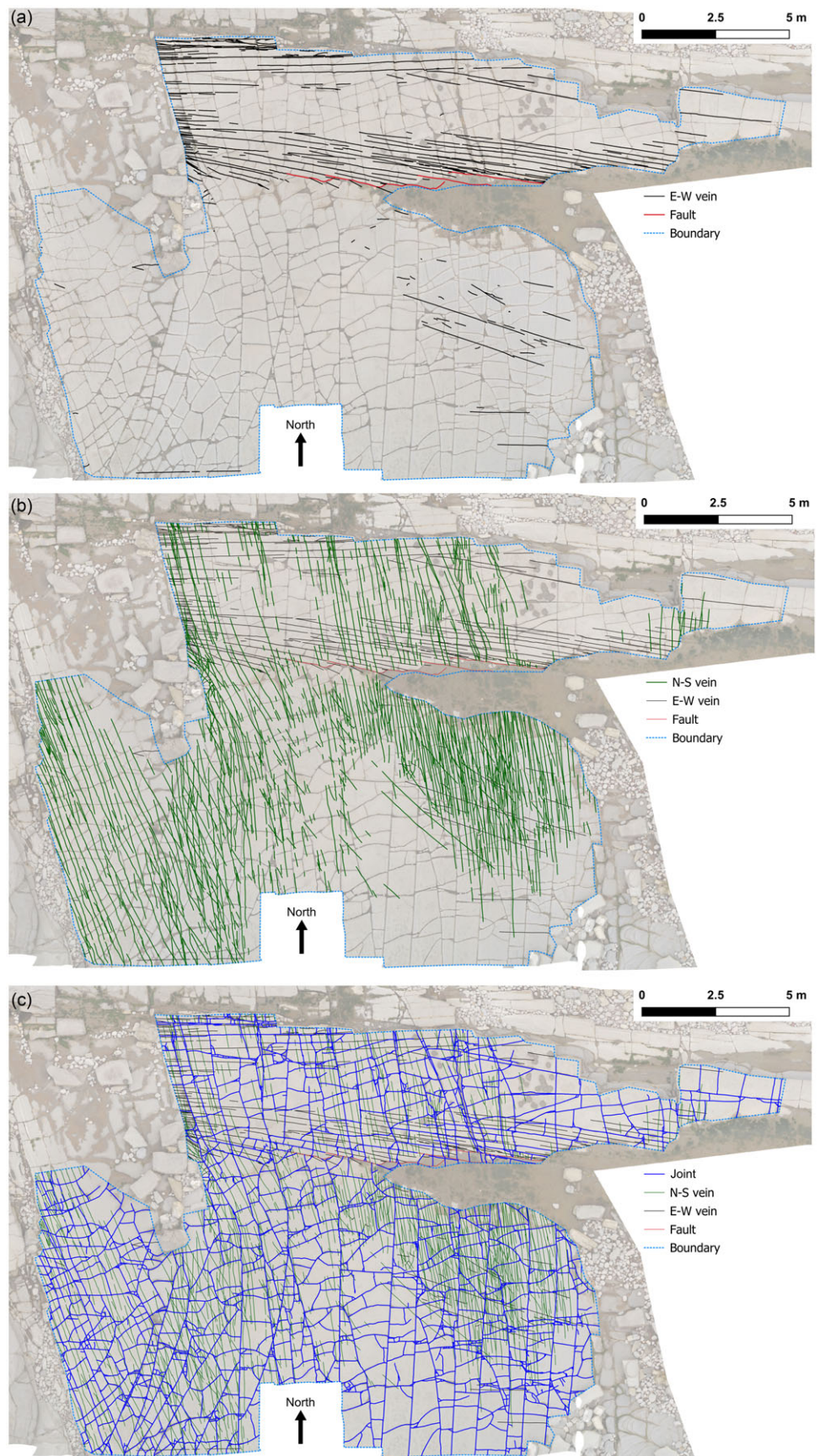


Figure 6. (Colour online) Maps of the different fracture sets at Lilstock. (a) Vein set A strikes approximately E-W and is clustered around a fault zone with an approximate E-W strike. (b) Vein set B strikes approximately N-S to NW-SE and are clustered around faults that strike approximately NNW-SSE. Veins of set B cross-cut or trail through veins of set A. (c) A network of joints is superposed on the pre-existing veins. Some joints cross-cut the veins, while other follow (reactivate) the veins.

suggests that it may be possible to further divide veins of this orientation on the basis of orientation and relative ages.

5.b. Joint networks

The joints show the following characteristics:

- **Orientations.** The joints dip at $\sim 90^\circ$ to bedding and their strikes are shown in Fig. 5c, d. Two orientations of joint appear to dominate, these being \sim N-S and \sim E-W. The joints that follow veins have, however, the same orientations as vein sets A and B. The sets have a much less clearly defined preferred orientation than the veins, with only $\sim 80\%$ of the data within broad orientation ranges that occupy $\sim 70\%$ of the total range. Many of the joints curve, creating problems for subdividing the joints into sets based purely on their orientation (e.g., Engelder & Delteil, 2004). For simplicity, we consider the entire joint network to be simply one set, based only on fracture type.
- **Apertures.** The joints generally show sub-millimetre apertures. Some wider joints occur, and this probably is caused by weathering and erosion.
- **Trace lengths.** The maximum trace length measured for the joints is at least 8.98 m, with this longest joint extending to the edge of the mapping area. The mean length is ~ 0.53 m ($n = 1881$). The joints show a mean trace length per unit area of ~ 4.4 m $^{-1}$.
- **Geometric indicators of kinematics.** Joints tend to show opening-mode displacement (e.g., Pollard & Aydin, 1988), but curvature along many of the joints may suggest a component of shear along portions of such joints.
- **Distributions.** The joints appear to be fairly evenly distributed across the mapped area, with some appearing to curve into fault zones (Fig. 6c). Such behaviours for joints in the Liassic rocks of the Bristol Channel Basin are described by Rawnsley *et al.* (1992, 1998) and Bourne and Willemse (2001). The veins appear to be clustered around faults, so the joints that follow veins are also spatially related to faults.
- **Relationships with veins.** The joints either cross or follow both sets of veins. The joints that follow the veins do not seem to extend to and beyond the tips of those veins, suggesting that vein aperture is important in controlling whether or not a vein will be reactivated as a joint.
- **Relationships between joints.** Pairs of joints in the Liassic rocks of the Somerset coast typically show abutting relationships (e.g., Rawnsley *et al.*, 1998; Peacock *et al.*, 2018). Some crossing relationships occur where one or both joints follow veins.
- **Relative ages.** The joints cross-cut or follow vein sets A and B, so post-date the veins. Abutting relationships between joints would enable relative ages of different joints (or joint sets) to be determined (e.g., Peacock *et al.*, 2018). Hancock and Engelder (1989) suggest that many joints in northwestern Europe were created by exhumation in a regional stress field in which maximum horizontal compressive stress was orientated \sim NW-SE.

5.c. Veins and joints combined

Orientation data for the combined populations of veins and joints (Fig. 5e, f) show intermediate behaviour between the orientations of the veins and of the joints independently. Approximately 57.7%

of the fracture lengths (veins and joints combined) fall in the strike range of 145° – 185° , while approximately 28% of the fracture lengths fall in the strike range of 060° – 105° .

6. Topologies of superposed fracture networks at Lilstock

Any network in two dimensions, such as fracture traces, can be represented by a system of nodes and branches (Sanderson & Nixon, 2015). The branches represent the fracture traces and the nodes record information about the types and distributions of intersections between the fractures. Topology emphasizes the relationships between two or more individual structures, such as crossing and abutting relationships of fractures (e.g., Sanderson & Nixon, 2015; Peacock *et al.*, 2017, 2018). Network topology is useful for characterizing many aspects of fracture networks (e.g., Sanderson & Nixon, 2015; Duffy *et al.*, 2015; Procter & Sanderson 2018), including establishing the relative age of different structures. It is also useful for understanding the connectivity of fractures within a network (e.g., Berkowitz *et al.*, 2000; Manzocchi, 2002; Sanderson & Nixon, 2018). Here, we use the node types shown by the different components of the fracture network at Lilstock to show how these differentiate different forms of superposition.

6.a. Vein network

The vein network consists of two sets. Veins in Set A (the older set) are commonly isolated or show *en echelon* relationships. Set A is dominated by I-nodes (Table 2a, Figs. 6a, 7), which form 92.3% of the nodes. They also have a strong spatial clustering around the faulted margin of the exposed bedding plane.

Veins in Set B (the younger set of veins) appear to form swarms, with *en echelon* patterns being less common (Fig. 6b). The Vein B network is still dominated by I-nodes (77.4%), but with significantly more Y- and X-nodes (Table 2). X-nodes are created by cross-cutting relationships between veins in Set B (\sim NNW-SSE striking veins appear to cross-cut \sim N-S striking veins).

Set B is superposed on Set A creating a higher proportion of X-nodes because the two sets cross (Table 2a, all veins). The two sets of veins combined still shows a majority of I-nodes (52.4%), with 31.5% of the nodes being X-nodes (Table 2a, Fig. 7) at which Set B is seen to cut Set A.

Both Set A and Set B veins develop in damage zones related to two different generations of faults, and this spatial clustering results in limited connectivity across the exposure, with a high proportions of I-nodes. Where superposition occurs, Set A veins are generally overprinted by Set B, producing almost four times as many X-nodes as Y-nodes.

6.b. Joint networks

The joint network is dominated by Y-nodes, these forming 84.6% of the nodes and 94% of the connected nodes (Table 2a, Fig. 7). Prabhakaran *et al.* (2021) report that Y-nodes form 70 to 80% of the nodes in Liassic limestones ~ 2.3 km to the east at Lilstock. I-nodes are rare (10.3%; Table 2a), with the joints being highly connected in the network. Six V-nodes were identified, but these are not included in the analysis.

A key feature that distinguished the topology of the joint network is the dominance of Y-nodes, indicating that joints nucleate and/or terminate against one another, which is often termed abutment. This strong interaction contrasts with the cross-cutting and overprinting seen within the vein network. We will

Table 2. Node types for the superposed fracture network at Lilstock. (a) Numbers (and percentages) of node types for the components. % C = the percentages of connected nodes (i.e., percentage of Y-, X- and Z-nodes). (b) Numbers (and percentages) of connected node types at interactions between different components

	I	Y	X	N	% I	% Y	% X	% C	
(a)									
Set A veins	525	0	39	5	569	92.3%	6.9%	0.9%	7.7%
Set B veins	1593	0	294	170	2057	77.4%	14.3%	8.3%	22.6%
All veins	1953	0	602	1174	3729	52.4%	16.1%	31.5%	47.6%
Joints	350	6	2876	168	3400	10.3%	84.6%	4.9%	89.7%
All fractures	2022	1	3444	4021	9488	21.3%	36.3%	42.4%	78.7%
Interactions									
			Y					X	
(b)									
Vein:Vein			602 (33.9%)					1174 (66.1%)	
Set A:Set B			269 (21.2%)					999 (78.8%)	
Joint:Vein			593 (17.9%)					2728 (82.1%)	
Joint:Joint			2876 (94.5%)					168 (5.5%)	

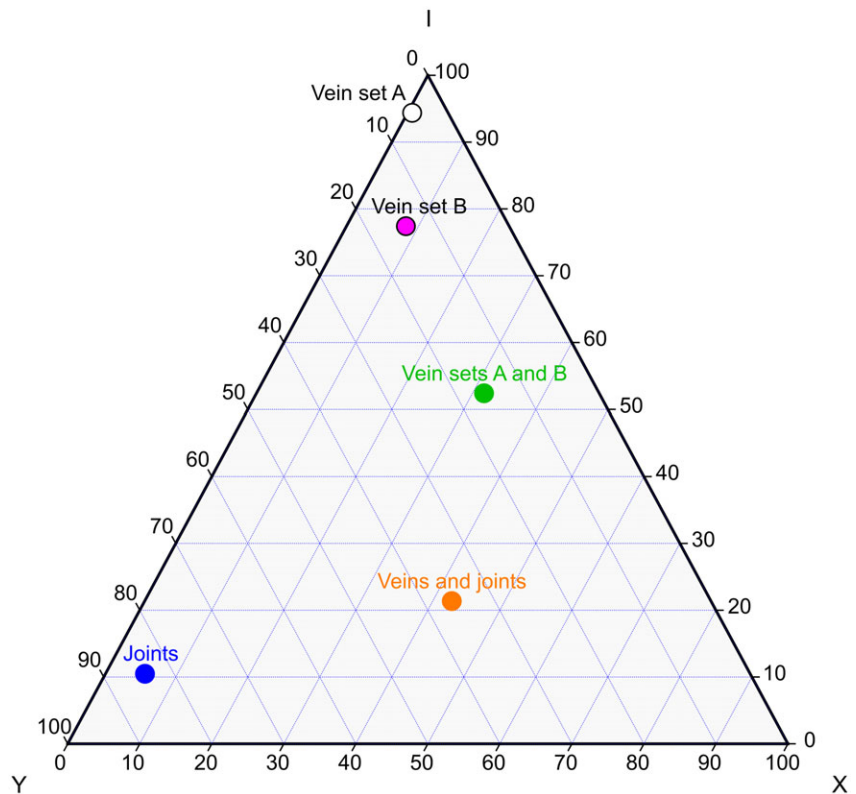


Figure 7. (Colour online) Ternary plot of I-, Y- and X-nodes for the veins, the joints and both the veins and joints combined. The vein network is dominated by I-nodes, with more X-nodes than Y-nodes. The joint network is dominated by Y-nodes. The veins and joints combined are dominated by Y- and X-nodes.

examine the interactions between the vein and joint network in the next section.

6.c. Combined network of veins and joints

Combining data for all of the veins and the joints produce a superposed network, with orientations intermediate between the veins and the joints (Fig. 5). At the resolution mapped, the total superposed network has a fracture intensity of just over 10 m^{-1} , with the joints forming 42.4% of this (Table 1). The topology of the combined network (Fractures in Table 2a) is different from either

the veins or the joints and cannot be predicted simply from the weighted average of the two networks. The superposed network contains a significantly higher proportion of X-nodes (42.4%) (Table 2a, Fig. 7). We can use the node counts to test hypotheses about the character of the interaction between the two networks.

The data for the connected nodes (Y- and X-nodes) in the vein and joint networks are extracted from Table 2a and combined with data on the number of connected nodes for Set A and Set B intersections and for those between the joints and veins (Table 2b). The proportions of X- and Y-nodes vary between the different types of intersections. Y-nodes dominate (94.5%) for joint:joint

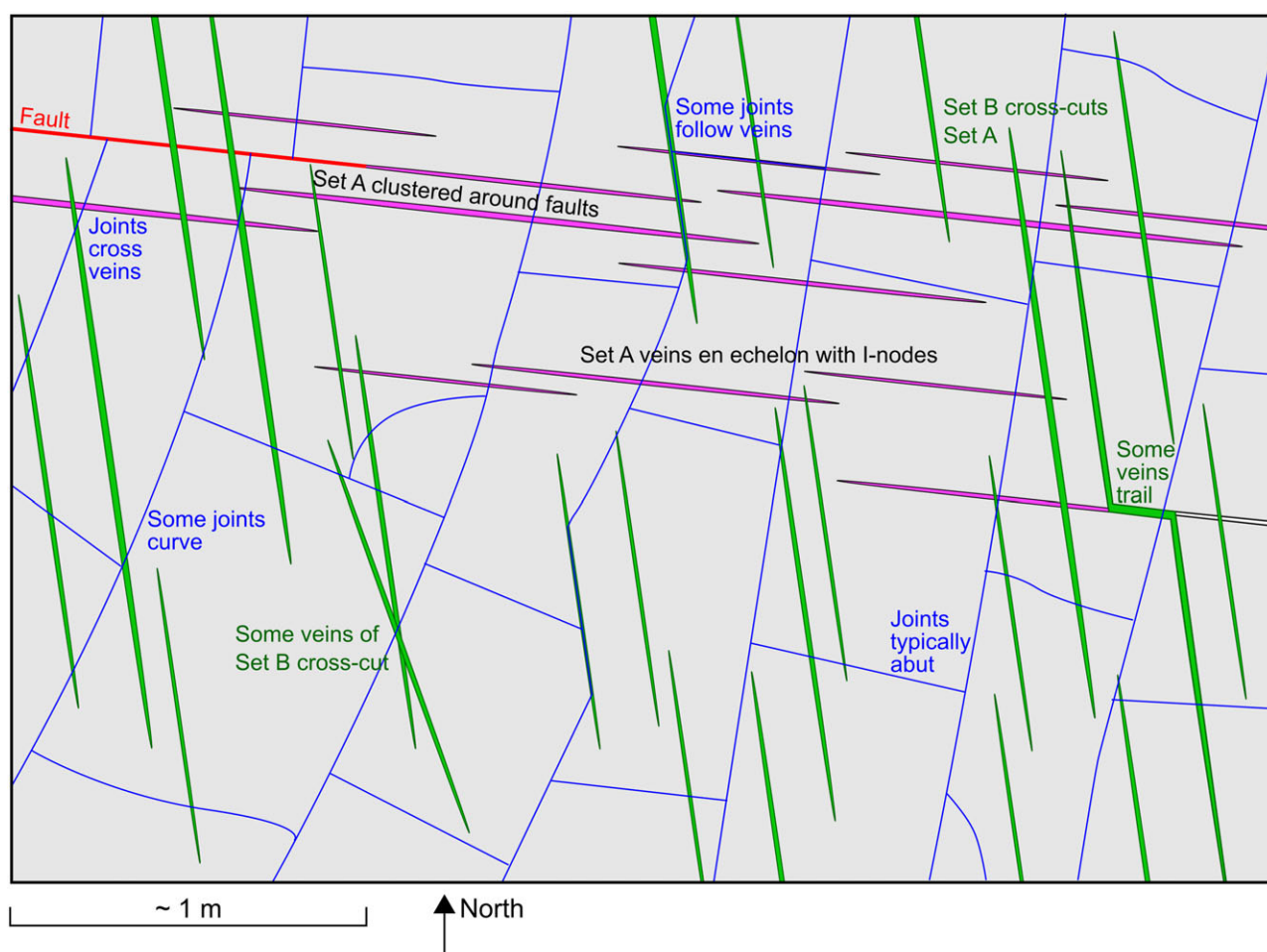


Figure 8. (Colour online) Schematic model for the superposition of the fracture network at Lilstock. Vein set A is clustered around a fault, with these veins typically being *en echelon* and forming I-nodes. Vein set B crosses vein set B to form X-nodes, although some trail through veins of Set A. The joints form a later network that cut across or follow veins of sets A and B. Later joints typically abut earlier joints.

intersections, whereas X-nodes dominate (82.1%) for joint:vein intersections. The vein:vein intersections are also dominated by X-nodes but to a somewhat lesser extent (66.1% for all intersections and 78.8% for Set A:B intersections). Table 2a is a simple contingency table with almost zero probability of a random distribution of node types. These data strongly support the idea that vein Set A is overprinted by Set B, but interaction of the joints and veins is more complex. The joints both cross-cut the veins (high % of X-nodes) but also run along (and reactivate) the veins, suggesting both overprinting and utilization of the pre-existing network. The joints dominantly abut other joints, either initiating or terminating at pre-existing joints producing mainly Y-nodes.

7. Discussion

A schematic model for the development of the vein and joint network at Lilstock is shown in Fig. 8. Here, we discuss aspects of the analysis and development of this and other superposed fracture networks.

7.a. Evolution

The analysis presented here enables the following evolution of the fracture network to be determined. Note that *connectivity* refers to the degree to which fractures are connected within a network,

which depends on the size, frequency, orientation, spatial correlation, scaling and topology (Berkowitz *et al.*, 2000; Manzocchi, 2002). Three main stages can be identified (Figs. 6, 8):

- *Stage 1:* development of vein Set A, in the damage zones of ~ E-W-striking normal or oblique-slip faults (Fig. 6a). At this stage, the veins are mostly localized adjacent to the faults that bound the area, with little connectivity across the exposed bedding plane.
- *Stage 2:* development of vein Set B, in the damage zones of ~ NW-SE-striking strike-slip faults (Fig. 6b). Some of veins in Set B trail through veins in Set A, while others cross to form X-nodes. At this stage, there was limited connectivity between the Set B veins, but the total vein network is weakly connected across the exposed area.
- *Stage 3:* development of the joint network (Fig. 6c). The joints reactivate (follow), trail through or cross-cut the earlier veins. The joint network itself is well connected, mainly through Y-nodes, with few I-nodes. The joint network overprints and reactivates the vein network to produce a superposed vein-joint network that is well-connected network.

The sequential evolution of network connectivity has been documented by Park *et al.* (2010). Determining this evolution

Table 3. Examples of different types of fault reactivation

Reactivation type	Example	Reference
Normal as reverse	Lillecombe Down, Isle of Wight, UK	Underhill and Paterson (1998)
Normal as strike-slip	Garmonda and Tormeno faults, Italian Alps	Zampieri and Massironi (2007)
Reverse as normal	Camargue and Western Provencal basins, France	Mauffret and Gorini (1996)
Reverse as strike-slip	Hangjinqi fault zone, China	Yang <i>et al.</i> (2013)
Strike-slip as normal	Sante Marie-Tagliacozzo and Colli di Monte Bove-Roccamerco faults, central Italy	Frepoli <i>et al.</i> (2010)
Strike-slip as reverse	Synclinal Median fault, French Alps	Guillot <i>et al.</i> (2009)

Table 4. Examples of different types of fracture reactivation

Reactivation type	Example	Reference
Shear as extensional	Igneous intrusion along a fault, Hekla Fissure, Iceland	Gudmundsson (2007)
Shear as compactional	Pressure solution along normal faults, Flamborough Head, UK	Peacock <i>et al.</i> (1998)
Extensional as shear	Faulted joints, Arches National Park, USA	Cruikshank <i>et al.</i> (1991)
Extensional as compactional	Joints reactivated as slickolites, Holderbank quarry, northern Switzerland	Ramsay and Huber (1987)
Compactional as shear	Sheared stylolites, Majella Mountain, Italy	Tondi <i>et al.</i> (2006)
Compactional as extensional	Veining along opened stylolites, SE Basin, France	Micarelli <i>et al.</i> (2005)

requires both identification of the types of fracture involved and examination of their relationships (reactivation, trailing, crossing, etc.).

7.b. Overprinting and reactivation

The superposition of two or more fracture networks can occur in different ways. The N-S veins largely overprint the E-W veins, producing cross-cutting intersections (high proportion of X-nodes in Table 2), with a limited amount of reactivation, as indicated by occasional trailing. The joint network shows both overprinting, abutting (Y-nodes) and much re-utilization of the earlier formed veins (joints along veins), with abundant termination and trailing of joints at veins and particularly at earlier formed joints.

Fracture reactivation is a common form of superposition. Faults are commonly reactivated with a different sense of displacement, with examples given in Table 3. This reactivation can be a component of fracture network superposition. For example, Kelly *et al.* (1999) show that reverse-reactivation of E-W-striking normal faults in the Liassic rocks at East Quantoxhead (~5 km WSW of the study area at Lilstock) was accompanied by the development of a network of conjugate strike-slip faults. Fracture network superposition can also involve fractures being reactivated as other types of fractures, such as an extension fracture (e.g., a vein or a joint) being reactivated as a contractional structure (e.g., a stylolite). Examples of such reactivation are given in Table 4.

7.c. Implications for analysing and understanding fracture networks

Just as understanding superposed folding helps unravel the deformation history of a region (e.g., Ray, 1974; Ramsay & Huber, 1987), understanding superposition in fracture networks helps determine the evolution of that network. Rather than analysing the final fracture network as a single entity (e.g., Zhu *et al.*, 2022), it is necessary to distinguish the different fracture

types present and determine the sequence of development of the components of the network (e.g., Katternhorn *et al.*, 2000; Gillespie *et al.*, 2001), if the geometric and topological development of the network is to be understood. This involves using geometric and topological characteristics to define different classes or ages of fracture that are appropriate for the study (e.g., Peacock & Sanderson, 2018; Andrews *et al.*, 2020). Such an approach helps deduce how fractures have been controlled by the interplay between palaeostress fields and earlier structures and would lead to better understanding of the kinematic, tectonic and fluid flow history. Simply adding all fractures together in a network would be analogous to not distinguishing between paths, roads, canals, railways and aeroplane flight paths, and lumping them all together to analyse a transport network.

7.d. Other network components and examples

While we have focused on a fracture network created by the superposition of two sets of veins and a joint network, the analysis can be expanded to include other structures in the network. For example, some of the stepping veins of Set B are linked by stylolites or slickolites, with some forming pull-aparts (e.g., Willemsse *et al.*, 1997). At a larger scale, the two vein sets appear to be damage related to a network of superposed faults (Fig. 3). Superposed fault networks can show abutting (e.g., Nixon *et al.*, 2014, Fig. 11), crossing (e.g., Dart *et al.*, 1995; Gonzalo-Guerra *et al.*, 2023), reactivating (Table 3) or trailing (Nixon *et al.*, 2014, Fig. 15) relationships.

8. Conclusions

Superposed fracture networks result from the successive development of different ages (and commonly different types) of fractures. Successive sets of fractures may either overprint (cross-cut), follow (reactivate) or arrest at (abut) the earlier ones. In the example of veins and joints on a Liassic limestone bedding plane at Lilstock,

UK, the network comprises (1) early formed E-W veins, (2) later N-S veins and (3) a later system of joints. The later components of a superposed fracture network can both overprint and re-utilize (reactivate) earlier fractures. For example, the N-S veins at Lilstock cross-cut and trail into E-W veins, and the joints abut, cross-cut and reactivate both the vein sets.

The different components of a superposed fracture network can have different topologies. The first set of veins at Lilstock is dominated by I-nodes, with linkage of the straight, sub-parallel veins being limited. The second set of veins is still dominated by I-nodes, but locally cross-cut Set A, producing more X-nodes. The joints cross-cut both sets of veins, producing X-nodes. This indicates overprinting of the vein network by joints, but that some utilizing earlier veins as they develop. Joint:joint intersections are dominantly Y-nodes, indicating strong mechanical interaction during joint development.

When interpreting a superposed fracture network, it is important to separate out the components, based on both the type of fracture and their age relationships. Although we have focused on veins and joints, this type of analysis is applicable to other types of superposed fracture networks, including faults.

Acknowledgements. M. Magán was supported by a Severo Ochoa grant and project AYUD/2021/51293 funded by the Government of Asturias and by Research project PID2021-126357NB-I00 funded by the Spanish Ministry of Science and Innovation. We thank Billy Andrews, Tom Blenkinsop and an anonymous reviewer for their useful comments.

Competing interests. The authors declare none.

References

- Andrews BJ, Shipton ZK, Lord R and McKay L (2020) The growth of faults and fracture networks in a mechanically evolving, mechanically stratified rock mass: a case study from Spireslack Surface Coal Mine, Scotland. *Solid Earth* **11**, 2119–40.
- Belayneh M, Masihi M, Matthäi SK and King PR (2006) Prediction of vein connectivity using the percolation approach: model test with field data. *Journal of Geophysics and Engineering* **3**, 219–29.
- Berkowitz B, Bour O, Davy P and Odling N (2000) Scaling of fracture connectivity in geological formations. *Geophysical Research Letters* **27**, 2061–4.
- Biddle KT and Christie-Blick N (1985) Glossary – strike-slip deformation, basin formation, and sedimentation. In *Strike-Slip Deformation, Basin Formation, and Sedimentation* (eds KT Biddle & N Christie-Blick), pp. 375–86. Claremore, Oklahoma: Society of Economic Paleontologists and Mineralogists, Special Publication 37.
- Bourne SJ and Willemse EJM (2001) Elastic stress control on the pattern of tensile fracturing around a small fault network at Nash Point, UK. *Journal of Structural Geology* **23**, 1753–70.
- Caputo R and Hancock PL (1998) Crack-jump mechanism of Microvein formation and its implications for stress cyclicity during extension fracturing. *Journal of Geodynamics* **27**, 45–60.
- Chen J (2013) Normal fault patterns and their rationality analysis. *Geophysical Prospecting for Petroleum* **52**, 201–6.
- Craw D, Upton P, Yu BS, Horton T and Chen YG (2010) Young orogenic gold mineralisation in active collisional mountains, Taiwan. *Mineralium Deposita* **45**, 631–46.
- Cruikshank KM, Zhao G and Johnson AM (1991) Analysis of minor fractures associated with joints and faulted joints. *Journal of Structural Geology* **13**, 865–86.
- d'Ars JDB and Davy P (1991) Gravity instabilities in magma chambers: rheological modelling. *Earth and Planetary Science Letters* **105**, 319–29.
- Dart CJ, McClay K and Hollings PN (1995) 3D analysis of inverted extensional fault systems, southern Bristol Channel basin, U.K. In *Basin Inversion* (eds JG Buchanan & PG Buchanan), pp. 393–413. Bath, UK: Geological Society of London, Special Publication no. 88.
- Deng H and McClay K (2021) Three-dimensional geometry and growth of a basement-involved fault network developed during multiphase extension, Enderby Terrace, North West Shelf of Australia. *Geological Society of America Bulletin* **133**, 2051–78.
- Dershowitz WS (1984) Rock Joint Systems. PhD thesis, Massachusetts Institute of Technology, USA, 918 pp.
- Drobe J, Lindsay D, Stein H and Gabites J (2013) Geology, mineralization, and geochronological constraints of the Mirador Cu-Au Porphyry District, southeast Ecuador. *Economic Geology* **108**, 11–35.
- Duffy OB, Bell RE, Jackson CAL, Gawthorpe RL and Whipp PS (2015) Fault growth and interactions in a multiphase rift fault network: Horda Platform, Norwegian North Sea. *Journal of Structural Geology* **80**, 99–119.
- Engelder T and Dellel J (2004) The orientation distribution of single joint sets. In *The Initiation, Propagation, and Arrest of Joints and Other Fractures* (eds JW Cosgrove & T Engelder), pp. 285–297. Bath, UK: Geological Society of London, Special Publication no. 231.
- Evans MA (1994) Joints and décollement zones in Middle Devonian shales: evidence for multiple deformation events in the central Appalachian Plateau. *Geological Society of America Bulletin* **106**, 447–60.
- Forstner SR and Laubach SE (2022) Scale-dependent fracture networks. *Journal of Structural Geology* **165**, 104748.
- Frepoli A, Marra F, Maggi C, Marchetti A, Nardi A, Pagliuca NM and Pirro M (2010) Seismicity, seismogenic structures, and crustal stress fields in the greater Rome area (central Italy). *Journal of Geophysical Research* **115**, B12303.
- Gillespie PA, Walsh JJ, Watterson J, Bonson CG and Manzocchi T (2001) Scaling relationships of joint and vein arrays from The Burren, Co. Clare, Ireland. *Journal of Structural Geology* **23**, 183–201.
- Glen RA, Hancock PL and Whittaker A (2005) Basin inversion by distributed deformation: the southern margin of the Bristol Channel Basin, England. *Journal of Structural Geology* **27**, 2113–34.
- Gonzalo-Guerra B, Heredia N, Farias P, García-Sansegundo J and Martín-González F (2023) Superimposed brittle structures in polyorogenic contexts: Variscan and Alpine faults in the Duje Valley (Picos de Europa, Cantabrian Mountains, NW Spain). In *Geological Mapping of Our World and Others* (eds RWH Butler, T Torvela & L Williams): Geological Society of London, Special Publication no. 541. doi: [10.1144/SP541-2022-276](https://doi.org/10.1144/SP541-2022-276).
- Gorodnitskiy AM, Filin AM, Malyutin YD, Ivanenko AN and Shishkina NA (2009) Southern Barents Sea anomalous magnetic field and its correlation with bottom geological structure. *Earth Science Frontiers* **16**, 240–7.
- Guastoni A, Pennacchioni G, Pozzi G, Fioretti AM and Walter JM (2014) Tertiary pegmatite dikes of the central Alps. *The Canadian Mineralogist* **52**, 191–219.
- Gudmundsson A (2007) Infrastructure and evolution of ocean-ridge discontinuities in Iceland. *Journal of Geodynamics* **43**, 6–29.
- Guillot S, di Paola S, Ménot RP, Ledru P, Spalla MI, Gosso G and Schwartz S (2009) Suture zones and importance of strike-slip faulting for Variscan geodynamic reconstructions of the External Crystalline Massifs of the western Alps. *Bulletin de la Société Géologique de France* **180**, 483–500.
- Hancock PL (1985) Brittle microtectonics: principles and practice. *Journal of Structural Geology* **7**, 437–57.
- Hancock PL and Engelder T (1989) Neotectonic joints. *Geological Society of America Bulletin* **101**, 1197–208.
- Hanks CL, Wallace WK, Atkinson PK, Brinton J, Bui T, Jensen J and Lorenz J (2004) Character, relative age and implications of fractures and other mesoscopic structures associated with detachment folds: an example from the Lisburne Group of the northeastern Brooks Range, Alaska. *Bulletin of Canadian Petroleum Geology* **52**, 121–38.
- Kattenhorn SA, Aydin A and Pollard DD (2000) Joints at high angles to normal fault strike: an explanation using 3-D numerical models of fault-perturbed stress fields. *Journal of Structural Geology* **22**, 1–23.
- Kelly PG, Peacock DCP, Sanderson DJ and McGurk AC (1999) Selective reverse-reactivation of normal faults, and deformation around reverse-reactivated faults in the Mesozoic of the Somerset coast. *Journal of Structural Geology* **21**, 493–509.

- Lee CH, Yu JL and Hwung HH (1993) Fluid flow and connectivity in fractured rock. *Water Resources Management* 7, 169–84.
- Lewis H, Couples G, Tengattini A, Buckman J, Tudisco E, Etxegarai M, Viggiani G and Hall SA (2023) Interactions between imbibition and pressure-driven flow in a microporous deformed limestone. *Transport in Porous Media* 146, 559–85.
- Lindström M (1961) On the significance of β intersections in superposed deformation fabrics. *Geological Magazine* 98, 33–40.
- Manzocchi T (2002) The connectivity of two-dimensional networks of spatially correlated fractures. *Water Resources Research* 38, 1162.
- Marrett R (1996) Aggregate properties of fracture populations. *Journal of Structural Geology* 18, 169–78.
- Mauffret A and Gorini C (1996) Structural style and geodynamic evolution of Camargue and Western Provencal basin, southeastern France. *Tectonics* 15, 356–75.
- Micarelli L, Benedicto A, Invernizzi C, Saint-Bezar B, Michelot JL and Vergely P (2005) Influence of P/T conditions on the style of normal fault initiation and growth in limestones from the SE-Basin, France. *Journal of Structural Geology* 27, 1577–98.
- Nekrasov YM (1975) Structural types of gold-ore deposits occurring in variously deformed sandstone-shale host rocks. *International Geology Review* 17, 272–83.
- Nixon CW, Sanderson DJ, Dee S, Bull JM, Humphreys R and Swanson M (2014) Fault interactions and reactivation within a normal fault network at Milne Point, Alaska. *American Association of Petroleum Geologists Bulletin* 98, 2081–107.
- Nortje GS, Oliver NHS, Blenkinsop TG, Keys DL, McLellan JG and Oxenburgh S (2011) New faults v. fault reactivation: implications for fault cohesion, fluid flow and copper mineralization, Mount Gordon Fault Zone, Mount Isa District, Australia. In *Geology of the Earthquake Source: A Volume in Honour of Rick Sibson* (eds Å Fagereng, VG Toy and JV Rowland), pp. 278–311. Bath, UK: Geological Society of London, Special Publication no. 359.
- Odling NE (1997) Scaling and connectivity of joint systems in sandstones from western Norway. *Journal of Structural Geology* 19, 1257–71.
- Park SY, Kim Y-S, Ryoo CR and Sanderson DJ (2010) Fractal analysis of the evolution of a fracture network in a granite outcrop, SE Korea. *Geosciences Journal* 14, 201–15.
- Passchier M, Passchier CW, Weismüller C and Urai JL (2021) The joint sets on the Lilstock Benches, UK. Observations based on mapping a full resolution UAV-based image. *Journal of Structural Geology* 147, 104332.
- Peacock DCP (2001) The temporal relationship between joints and faults. *Journal of Structural Geology* 23, 329–41.
- Peacock DCP and Sanderson DJ (1999) Deformation history and basin-controlling faults in the Mesozoic sedimentary rocks of the Somerset coast. *Proceedings of the Geologists Association* 110, 41–52.
- Peacock DCP and Sanderson DJ (2018) Structural analyses and characterising fracture networks: seven pillars of wisdom. *Earth-Science Reviews* 184, 13–28.
- Peacock DCP, Fisher QJ, Willemsse EJM and Aydin A (1998) The relationship between faults and pressure solution seams in carbonate rocks and the implications for fluid flow. In *Faulting, Fault Sealing and Fluid Flow in Hydrocarbon Reservoirs* (eds G Jones, QJ Fisher & RJ Knipe), pp. 105–15. Bath, UK: Geological Society of London, Special Publication no. 147.
- Peacock DCP, Nixon CW, Rotevatn A, Sanderson DJ and Zuluaga LF (2017) Interacting faults. *Journal of Structural Geology* 97, 1–22.
- Peacock DCP, Sanderson DJ and Rotevatn A (2018) Relationships between fractures. *Journal of Structural Geology* 106, 41–53.
- Phillips TB, Jackson CAL, Bell RE and Duffy OB (2018) Oblique reactivation of lithosphere-scale lineaments controls rift physiography – the upper-crustal expression of the Sorgenfrei-Tornquist Zone, offshore southern Norway. *Solid Earth* 9, 403–29.
- Pollard DD and Aydin A (1988). Progress in understanding jointing over the past century. *Geological Society of America Bulletin* 100, 1181–204.
- Potts GJ and Reddy SM (1999) Construction and systematic assessment of relative deformation histories. *Journal of Structural Geology* 21, 1245–53.
- Potts GJ and Reddy SM (2000) Application of younging tables to the construction of relative deformation histories-I: fracture systems. *Journal of Structural Geology* 22, 1473–90.
- Prabhakaran R, Urai JL, Bertotti G, Weismüller C and Smeulders DMJ (2021) Large-scale natural fracture network patterns: Insights from automated mapping in the Lilstock (Bristol Channel) limestone outcrops. *Journal of Structural Geology* 150, 104405.
- Procter A and Sanderson DJ (2018) Spatial and layer-controlled variability in fracture networks. *Journal of Structural Geology* 108, 52–65.
- Ramsay JG (1980) The crack-seal mechanism of rock deformation. *Nature* 284, 135–9.
- Ramsay JG and Huber MI (1987) *The Techniques of Modern Structural Geology. Volume 2: Folds and Fractures*. London: Academic Press, 391 pp.
- Rawnsley KD, Rives T, Petit JP, Hencher SR and Lumsden AC (1992) Joint development in perturbed stress fields near faults. *Journal of Structural Geology* 14, 939–51.
- Rawnsley KD, Peacock DCP, Rives T and Petit J-P (1998) Jointing in the Mesozoic sediments around the Bristol Channel Basin. *Journal of Structural Geology* 20, 1641–61.
- Ray SK (1974) Inversion of fold-hinge in superposed folding: an example from the Precambrian of central Rajasthan, India. *Precambrian Research* 1, 157–64.
- Reinhardt MC and Davison I (1990) Structural and lithologic controls on gold deposition in the shear zone-hosted Fazenda Brasileiro Mine, Bahia State, Northeast Brazil. *Economic Geology* 85, 952–67.
- Rives T, Rawnsley KD and Petit J-P (1994) Analogue simulation of natural orthogonal joint set formation in brittle varnish. *Journal of Structural Geology* 16, 419–29.
- Rotevatn A and Peacock DCP (2018) Strike-slip reactivation of segmented normal faults: implications for basin structure and fluid flow. *Basin Research* 30, 1264–79.
- Ryan JL, Lonergan L and Jolly RJH (2000) Fracture spacing and orientation distributions for two-dimensional data sets. *Journal of Geophysical Research* 105, 19305–20.
- Sanderson DJ and Nixon CW (2015) The use of topology in fracture network characterization. *Journal of Structural Geology* 72, 55–66.
- Sanderson DJ and Nixon CW (2018) Topology, connectivity and percolation in fracture networks. *Journal of Structural Geology* 115, 167–77.
- Sanderson DJ and Peacock DCP (2019) Measurement of geometry and linkage in vein arrays. *Journal of Structural Geology* 118, 104–13.
- Sanderson DJ and Peacock DCP (2020) Making rose diagrams fit-for-purpose. *Earth-Science Reviews* 201, 103055.
- Shephard-Thorn ER, Lake RD and Atitullah EA (1972) Basement control of structures in the Mesozoic rocks in the Strait of Dover region, and its reflexion in the certain features of the present land and submarine geology. *Philosophical Transactions of the Royal Society of London* 272, 99–113.
- Sibson RH (1985) A note on fault reactivation. *Journal of Structural Geology* 7, 751–4.
- Snow DT 1970. The frequency and apertures of fractures in rock. *International Journal of Rock Mechanics and Mining Sciences & Geomechanics Abstracts* 7, 31–40.
- Stanley RS (1974) Environment of deformation, Monkton Quartzite, Shelburne Bay, Western Vermont. *Geological Society of America Bulletin* 85, 233–46.
- Tondi E, Antonellini M, Aydin A, Marchegiani L and Cello G (2006) The role of deformation bands, stylolites and sheared stylolites in fault development in carbonate grainstones of Majella Mountain, Italy. *Journal of Structural Geology* 28, 376–91.
- Treagus SH (1995) Superposed deformations by Mohr construction. *Journal of Structural Geology* 17, 783–91.
- Underhill JR and Paterson S (1998) Genesis of tectonic inversion structures: seismic evidence for the development of key structures along the Purbeck-Isle of Wight Disturbance. *Journal of the Geological Society of London* 155, 975–92.
- Van Hoorn B (1987) The south Celtic Sea/Bristol Channel Basin: origin, deformation and inversion history. *Tectonophysics* 137, 309–17, 323, 326, 329–34.

- Vermilye JM and Scholz CH** (1995) Relation between vein length and aperture. *Journal of Structural Geology* **17**, 423–34.
- Virgo S, Abe S and Urai JL** (2013) Extension fracture propagation in rocks with veins: insight into the crack-seal process using discrete element method modeling. *Journal of Geophysical Research* **118**, 5236–51.
- Weiss LE** (1959) Geometry of superposed folding. *Geological Society of America Bulletin* **70**, 91–106.
- Wilkins SJ, Gross MR, Wacker M, Eyal Y and Engelder T** (2001) Faulted joints: kinematics, displacement–length scaling relations and criteria for their identification. *Journal of Structural Geology* **23**, 315–27.
- Willemse EJM, Peacock DCP and Aydin A** (1997) Nucleation and growth of strike-slip faults in limestone. *Journal of Structural Geology* **19**, 1461–77.
- Yang M, Li L, Zhou J, Qu X and Zhou D** (2013) Segmentation and inversion of the Hangjinqi fault zone, the northern Ordos basin (North China). *Journal of Asian Earth Sciences* **70–71**, 64–78.
- Zampieri D and Massironi M** (2007) Evolution of a poly-deformed relay zone between fault segments in the eastern Southern Alps, Italy. In *Tectonics of Strike-Slip Restraining and Releasing Bends* (eds WD Cunningham and P Mann), pp. 351–66. Bath, UK: Geological Society of London, Special Publication no. 290.
- Zhu W, He X, Santoso RK, Lei G, Patzek TW and Wang M** (2022) Enhancing fracture network characterization: a data-driven, outcrop-based analysis. *Computers and Geotechnics* **152**, 104997.
- Zulauf G** (1993) Brittle deformation events at the western border of the Bohemian Massif (Germany). *Geologische Rundschau* **82**, 489–504.